Postprint of: Klugmann M., Dąbrowski P., Mikielewicz D., Flow distribution and heat transfer in minigap and minichannel heat exchangers during flow boiling, Applied Thermal Engineering, Vol. 181 (2020), 116034, DOI: 10.1016/j.applthermaleng.2020.116034

Flow distribution and heat transfer in minigap and minichannel heat exchangers during flow boiling

Michał Klugmann, Paweł Dąbrowski[a], Dariusz Mikielewicz

Gdańsk University of Technology, Faculty of Mechanical Engineering, Department of Energy and Industrial Apparatus, Narutowicza 11/12, 80-233 Gdańsk, Poland, +48 58 347 2254

[a]email: pawel.dabrowski@pg.edu.pl

Nomenclature

A	-	area, m^2
C_p	-	specific heat of fluid, J/kgK
G	-	mass flux, kg/m^2s
h	-	specific enthalpy, J/kg
k	-	correction factor
l	-	section length, m
$\dot{m}$	-	mass flow rate, kg/s
P	-	pressure, Pa
Q	-	heat flow rate, W
$\dot{q}$	-	heat flux, W/m^2
Re	-	Reynolds number
T	-	temperature, K
W	-	section width, m
x	-	vapour quality
z	-	distance from the section inlet, m

Greek symbols

α	-	overall heat transfer coefficient, W/m^2K
ΔP	-	pressure drop, Pa
ΔT	-	temperature difference, K

Subscripts

avg	-	average
D-B	-	Dittus-Boelter correlation

exp	-	experimental
f	-	liquid
g	-	vapour
in	-	inlet
MS	-	Mikielewicz correlation
out	-	outlet
sat	-	saturation

Abbreviations

EDM	-	Electrical Discharge Machining
HTC	-	Heat Transfer Coefficient
ORC	-	Organic Rankine Cycle

Abstract:

The topic of boiling heat transfer in miniscale geometries has focused the ever increasing interest of researchers in recent years. However, most of the works are related to mini- and microchannels and much less to minigaps. Meanwhile, minigaps allow for more comprehensive experimental studies, i.e. flow visualisations due to the flat, two-dimensional configuration of the flow. The results of the experimental investigations of a model plate heat exchanger, composed of a single plate with a heat exchange surface of 0.1 m x 0.2 m, made of brass are presented. The working fluid is pure ethanol. Between the plate and the cover of the exchanger, 0.5 mm and 1.0 mm thick minigaps are arranged. The 0.5 mm minigap has been compared to an equivalent minichannel structure (a set of 50 parallel minichannels) with an equal cross-sectional area (rectangular 1 mm x 1 mm). An attempt to intensify the heat exchange by modifying the minigap wall was made. Two variants were tested to check the potential increase in the heat transfer coefficient and flow resistance. The section cover is transparent in order to simultaneously register the flow structures with the measurements. The heat is supplied using a water circuit, where the temperature and flow of the water can be regulated in a constant temperature water tank. The flow configuration of the exchanger is countercurrent, with the vertical flow of

ethanol from the bottom to the top. The inlet and outlet manifolds are arranged as trapezoidal (Z-type design). The authors have analysed the efficiency of heat transport and pressure drop depending on the system operating parameters. The visualisations are thoroughly analysed to better understand the process. The main advantages of the presented work are a direct comparison of minigap and minichannel structures while standardising all other parameters; an interesting application of a simple, passive heat transfer intensification method which resulted in the unification of the velocity fields in the minigap and reduced maldistribution.

Keywords:

minigap, pressure drop, heat transfer coefficient, visualisation, maldistribution, intensification

1. Introduction

Miniaturisation combined with increasing efficiency and increasing the amount of transported heat currently cover most technical fields. So, there is a demand for high performance and highly compact heat exchangers. To meet the high thermal requirements of many industries, phase change heat transfer (evaporation or condensation) and mini-geometries for heat exchangers were implemented [1]. The phenomena accompanying the flow in a single minichannel as well as the thermal parameters associated with them are widely described in the literature, and researchers have been dealing with them for many years [2–8]. Unfortunately, a single minichannel is not able to provide sufficient mass flow rate, and hence sufficient heat flow rate while maintaining reasonable pressure drops. Hence, minichannel heat sinks with multiple parallel channels are becoming more and more popular because they provide high heat transfer coefficients, compactness, and large heat flow rates while still maintaining acceptable pressure drops [9–13]. Nevertheless, parallel channels connected with common inlet and outlet manifolds provide different issues, e.g. flow maldistribution [14,15]. Some researchers' attention is focused on this undesirable phenomenon that can cause an

uneven temperature profile over the heat sink's surface [13,16], non-uniform phase distribution (in a multi-phase flow) in channels [17,18], the occurrence of hot spots [19,20], channel blockage [21] or higher pressure drops [22].

In addition to minichannels, the second mini-geometry that is promising in terms of thermohydraulic properties during flow boiling is a minigap [23]. Minigaps are geometries whose width is much greater than their depth, unlike minichannels in which both dimensions are comparable. No specific definition or width-to-depth ratio was found in the literature that proposes the moment of the channel-to-gap transition. There are fewer studies on the subject of minigap geometry than minichannels, especially studies that deal with the maldistribution phenomenon or its effects on temperature profile distribution [24–28]. Meanwhile, minigap heat sinks seem to show some advantages in relation to heat sinks with a set of parallel minichannels. The design is technically simpler and, from the application point of view, minigaps seem to be less sensitive to the working fluid's impurities.

Xia et al. [29] performed a series of numerical simulations using ANSYS Fluent 6.3 aimed at comparing the flow distribution and heat transfer characteristics in 30 parallel minichannels with different cross-sectional shapes, connected by various collectors (triangular, symmetry trapezoidal and rectangular) with different flow configurations (types I, C, Z) where the inlet and outlet are perpendicular to the flow direction in the manifolds. Studies have shown that fluid distribution is more uniform for a type I configuration and least uniform for type Z. It has been found that the flow is symmetrical for a type I configuration. The maximum temperature can be observed near the outlet from the minichannels. The authors proposed minichannel shapes that result in heat transfer intensification.

Pan et al. [10] conducted an experimental investigation on pressure drop characteristics in 14 parallel 0.15 mm x 0.25 mm rectangular microchannels. The working medium was deionised water. The authors visualised the two-phase flow in the channels and proposed correlation for the pressure drop. The influence of mass flux, heat flux and vapour quality on pressure drops and their oscillations

were examined. The results show that the ratio of heat to mass can approximately indicate the variation in the quality of the outlet thermodynamic equilibrium. The proposed correlation agrees well with the experimental data.

Another experimental study concerning 27 parallel rectangular microchannels (0.47 mm x 0.382 mm) and flow boiling of R134a have been conducted by Dalkılıç et al. [11]. The effects of mass flux, heat flux, saturation temperature and vapour quality on the heat transfer coefficient have been tested. The authors claimed that until a certain threshold of vapour quality, mass flux is ineffective in the heat transfer coefficient while above a certain value of vapour quality, the effect of heat flux becomes negligible. Also, a two-phase heat transfer coefficient correlation for multi-microchannel heat sinks was proposed.

Strąk et al. [7] investigated the heat transfer coefficient for various fluids flowing in a single minichannel (1.7 mm deep, 16 mm wide and 180 mm long) with a heated plate modified by vibration-assisted laser surface texturing on one side oriented with seven inclination angles (from 0° to 180° relative to the horizontal plane). The results show that the inclination angle influences the heat transfer characteristics but this dependence differs for various fluids.

Alam et al. [30] conducted experimental studies on the flow boiling of water in a 12.7 mm wide silicon microgap heat sink for ten different microgap depths (80 μm–1000 μm) to find the best range of microgap dimensions in terms of heat flux and pressure drop. The authors conducted experiments for mass fluxes ranging from 390 to 900 kg/m^{2}s at an imposed effective heat flux ranging from 0 to 70 W/cm^2. In addition to thermal parameter measurements, flow visualisation was carried out using a high-speed camera to illustrate the bubble characteristics in the boiling flow. The authors stated that the heat transfer coefficient increases with decreases of the microgap's depth and that for microgaps within the range of 100–500 μm, dryout takes place intensively. For microgap depths of 700 μm and above, the dominant flow regime at low heat fluxes is bubbly flow while slug/annular flow appears as the heat flux is increased.

Another experimental study from Alam and Lee [31] was conducted on an expanding silicon microgap heat sink. The working medium was also deionised water. The results of this study show that an expanding microgap results in better distribution of fluid (a more uniform wall temperature) than a straight microgap heat sink and intensifies the heat transfer coefficient. Nevertheless, too big an expansion causes a loss of the intensification effect. The authors emphasised that further systematic studies on microgap heat sinks are needed.

A new idea of combining both mini-geometries, namely microgaps and microchannels, was proposed by Mathew et al. [24]. The novel hybrid heat sink that consists of 40 parallel microchannels (12.5 mm long and 0.6 mm x 0.3 mm rectangular cross-section) and a 25 mm wide microgap (0.6 mm in depth) shows good thermohydraulic characteristics. It combines the advantages of microchannels with the advantages of microgaps, namely superior heat transfer performance, good boiling stability and a lower pressure drop compared to the straight microchannel heat sink.

Research that can be considered as an inspiration for the current work was conducted by Alam et al. [26]. The authors experimentally investigated the flow boiling heat transfer and pressure drop characteristics of deionised water flowing through the microgap and 30 parallel microchannels. Moreover, they have taken a closer look at the local hotspots, which are a consequence of the flow maldistribution effect. Results showed that the microgap heat sink gives a very promising heat transfer performance at high heat flux and low mass flux. Pressure drops are smaller in the microgaps compared to the microchannels. The authors claimed that microgaps are very promising in cooling systems. To expand the knowledge, current studies have been conducted for smaller mass fluxes and other heat fluxes. Moreover, the working medium is ethanol and it flows through the different gap and channels as in the work by Alam et al. [26]. The current authors also focused more on the flow maldistribution phenomenon and its effect on thermohydraulic characteristics.

This literature review shows that there are very few authors that investigate the thermal and hydraulic characteristics of minigap together with minichannel heat sinks. So, more careful and comparative studies are needed to advance the fundamental cognition of local heat transfer

coefficients and pressure drops in minigap and minichannel heat sinks. Most of the papers focused on microgaps deal with these mini-geometries for the cooling applications of electronic systems. Such heat sinks have small overall dimensions. The novelty of this study is the possible application of minigaps or minichannels in systems bigger than electronic systems, e.g. solar [32], ORC micro power plants [33], chemical and biological systems [34,35].

In the current work, the authors analysed the operation of two kinds of model plate heat exchangers, namely minigap or minichannel heat exchangers. A single plate is equipped with a minigap 0.1 m long and 0.2 m wide with a thickness of 0.5 and 1.0 mm or with a set of 50 rectangular minichannels with a 1 mm x 1 mm cross-section, which results in the same total cross-sectional area. Heat transfer coefficients and pressure drops are compared for both cases as a function of various parameters. An attempt to create simple, passive heat exchange intensification has been made.

2. Experimental setup and data reduction procedure

2.1. Test rig

The measuring system (Fig.1) is a closed loop with the test fluid forced through by a pump. The evaporator is a plate heat exchanger. On the working side, it is configured as a minigap or a set of 50 minichannels with inlet and outlet manifolds in a trapezoidal design, the so-called Z-type (Fig. 2). The heat is supplied by circulating water configured in a countercurrent flow. The condenser is a shell-and-tube water-cooled heat exchanger. The mass flow rate of the working medium is measured using a Coriolis flowmeter Sitrans FC mass 2100 Di 1.5. The inlet and outlet temperatures of the evaporator and condenser are measured using T-type thermocouples, and additionally, 12 temperatures of the heat exchanger's wall have been measured. The inlet and outlet pressures of an evaporator are measured using highly precise KELLER PAA/33X transmitters. At the same time, the boiling structures are recorded with a fast shutter speed camera through the transparent evaporator wall.

The purpose of the work was to study the impact of changes of parameters such as heat flux supplied to the evaporator (Q = 82 ÷ 560 W, $\dot{q}$ = 4.1 ÷ 28 kW/m^2), mass flow rate ($\dot{m}$ = 0.5 ÷ 4.6 g/s, G = 10 ÷ 92 kg/m^{2}s) of the working fluid and the presence of mechanical minigap wall modifications on heat exchange efficiency and the pressure drop in a model heat exchanger.

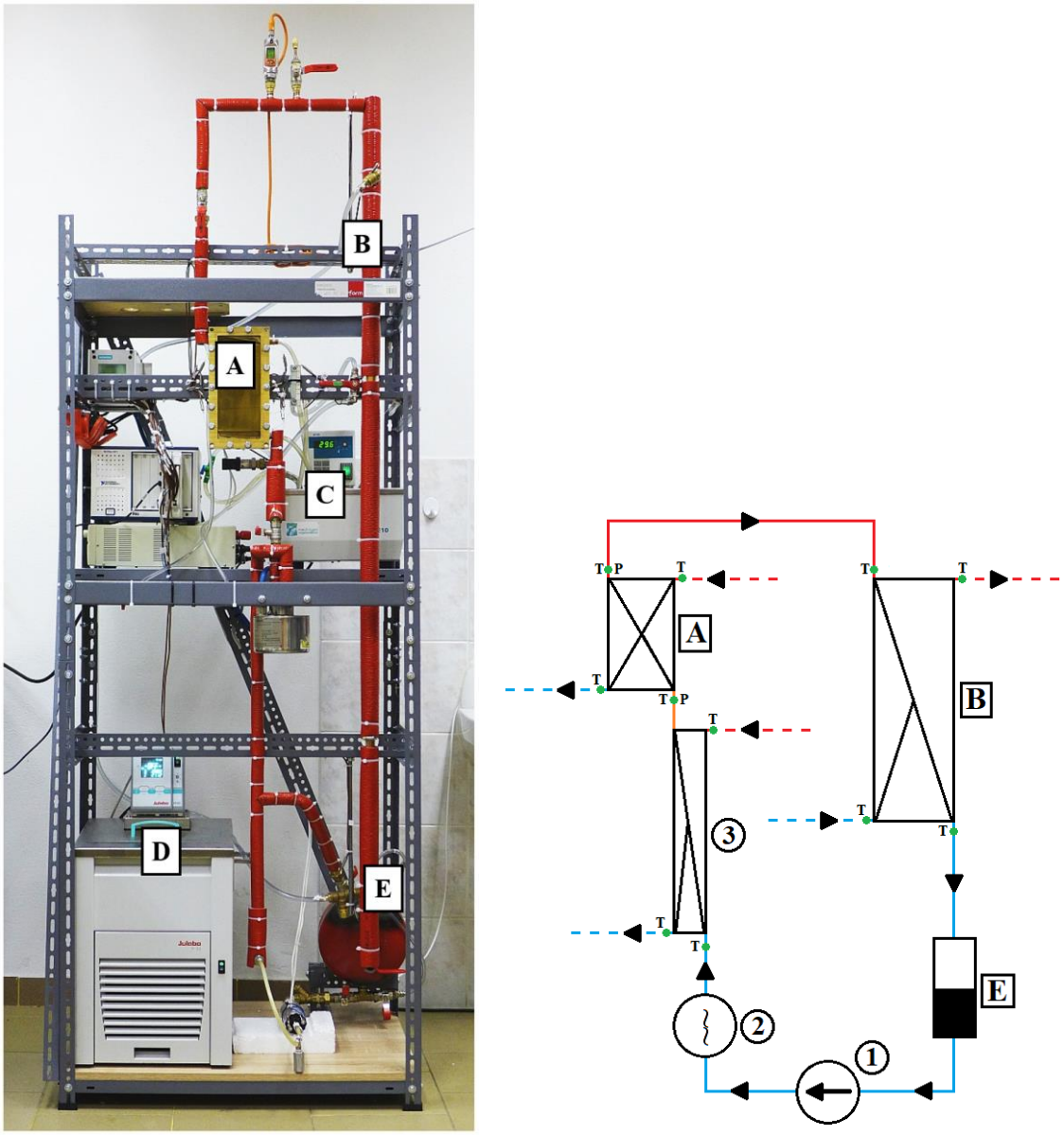

Fig. 1. Experimental rig: A – evaporator, B – condenser, C – heating constant temperature water tank, D – cooling constant temperature water tank, E – working fluid (ethanol) reservoir, 1 – circulation pump, 2 – mass flowmeter, 3 – pre-heater; solid line – ethanol flow, dashed line – heating/cooling water flow

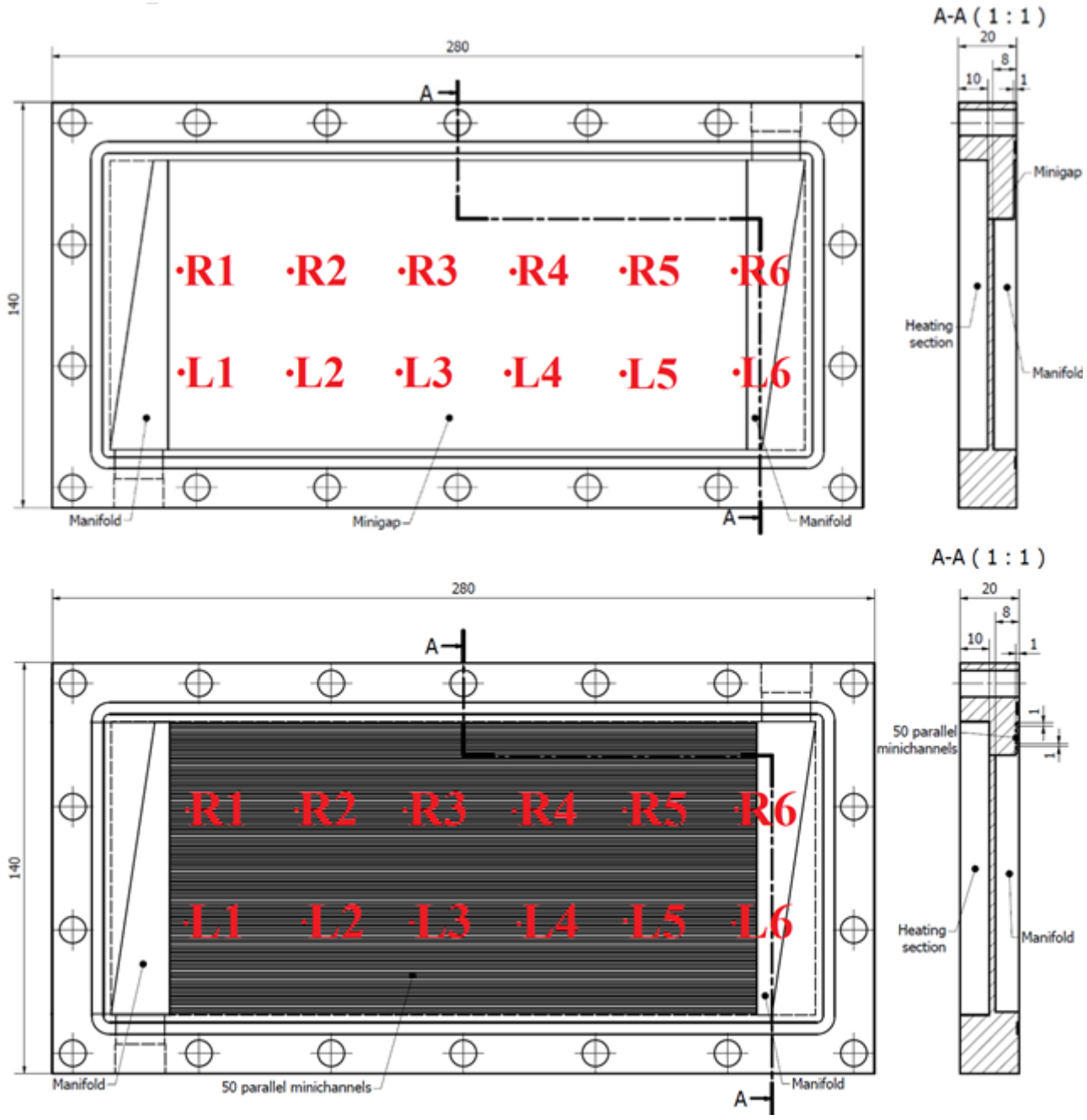

Fig. 2. Design of the minigap and minichannel evaporator plate (R, L – wall temperature measurement points)

The thermocouples for local wall temperature measurements are mounted in perpendicular ducts of 1 mm diameter, precisely drilled 1 mm below the heat exchange surface by the EDM method. The channels run across the entire width of the section, which allows any position of the thermocouples in the transverse dimension to be set. Before inserting the thermocouples, the ducts were filled with a thermally conductive paste to ensure adequate thermal contact. The authors calculated that the maximum temperature gradient at a thickness of 1 mm of brass is 0.25 K, which is less than the

nominal accuracy of a T-type thermocouple and can be neglected. All the thermocouples that measure the working fluid temperature have been mounted directly in the flow using special stuffing boxes.

2.2. Test procedure and data reduction

Measurement data are collected in series at variable mass fluxes of the working fluid and the other parameters fixed for a specific series. For the case of flow boiling, the working fluid is heated in the pre-heater to a temperature close to the saturation temperature. In this way, two-phase flow is obtained over the entire length of the measuring section (unless superheated steam eventually appears near the outlet). After leaving the measuring section, the medium is cooled back to room temperature and returns to the pre-heater. The mass flux of the ethanol is controlled by changing the voltage supplying the pump and using the by-pass.

During the measurement the following values are recorded with the following measurement error limits (Tab.1):

Tab. 1. Partial experimental uncertainties

Measurement	**Measuring range**	**Absolute error**	**Relative error**
Temperature (calibrated)	92 K	0.5 K	0.52%
Pressure	$7*10^4$ Pa	100 Pa	0.14%
Flow velocity – working fluid	$1.66*10^{-5}$ m^3/s	$4.16*10^{-7}$ m^3/s	2.5%
Flow velocity – pre-heating/heating/cooling circuit	$8.33*10^{-6}$ m^3/s	$2.5*10^{-7}$ m^3/s	3%
Linear dimensions	0.2 m	10^{-4} m	0.05%
Hydraulic diameter	0.013 m	10^{-4} m	0.76%

Using the uncertainty propagation method for error analysis, the total experimental error of heat flux is 3.64% and the overall heat transfer coefficient (HTC) does not exceed 4.68%.

The values of the HTC are derived using the equation which is a simple transformation of the test section heat balance, which can be seen in Eq. (1):

$$\alpha_{EXP} = k \cdot Q / (A \cdot \Delta T) \tag{1}$$

where: Q – the heat flow rate provided to the section; A – the area of the inner wall of test section; ΔT – the local temperature difference between the wall and the liquid (for convective heat exchange) or between the wall and the saturation temperature (for two-phase flow). Due to the lack of evaporator insulation, which is the result of the need for flow visualisation, the heat supplied to the evaporator and the heat taken in the condenser differ from each other. All temperatures and flow rates necessary for determining the heat balance were measured on the water heating side in the evaporator and the water cooling side in the condenser. The heat balance was calculated. The difference from the heat supplied to the evaporator and taken from the condenser is around 5%, so the k factor is 0.95. The heat flow rate provided to the section in single-phase flow can be calculated from Eq. (2) or, for the case of flow boiling from Eq. (3).

$$Q = \dot{m} \cdot Cp \cdot (T_{out} - T_{in}) \tag{2}$$

$$Q = \dot{m} \cdot (h_{out} - h_{in}) \tag{3}$$

The specific heat of the working medium is derived using the catalogue data supplied by the manufacturer; h_{out}, h_{in} – values read from tables for the measured temperature and pressure (in the case of liquid or overheated vapour) or the saturation temperature and vapour quality (in the case of two-phase flow). If the measuring point occurred in a single-phase heat transfer area, the local temperature of the fluid is calculated using a simple interpolation of the inlet and outlet temperature as shown in Eq. (4):

$$T_{(z)} = T_{in} + z / l \cdot (T_{out} - T_{in}) \tag{4}$$

where: z – the distance between the measuring point and the test section inlet; l – the length of the test section.

If the measuring point occurred in a flow boiling area, the local saturation temperature, determined using saturation pressure, is taken as the fluid temperature. The local pressure is calculated as a linear interpolation of the inlet and outlet pressure.

The local vapour quality is calculated from Eq. (5).

$$x_{(z)} = (h_{(z)} - h_f) / (h_g - h_f) \tag{5}$$

where: $h_{(z)}$ – the local specific enthalpy at a distance z from the section inlet; h_f – the specific enthalpy of the liquid; h_g – the specific enthalpy of the vapour.

The local specific enthalpy is calculated from Eq. (6).

$$h_{(z)} = h_{in} + (Q \cdot W \cdot z) / (A \cdot \dot{m}) \tag{6}$$

All the thermodynamic and transport properties were calculated using the REFPROP v9.0 program, developed by the National Institute of Standards and Technology (NIST). Temperature and pressure were measured at the preheater outlet (evaporator inlet) and evaporator outlet, so all the thermodynamic and transport properties were known at those points when it was single-phase flow. Moreover, the fluid at the outlet of the preheater was always in liquid phase near saturation, so the thermodynamics and transport properties were also known. The heat transferred to liquid in every part of the evaporator was known, so even in a two-phase flow region, all the thermodynamic and transport properties could be calculated.

3. Experimental results

3.1. Single-phase convective heat transfer

For the mass flux in the range of 2.4 ÷ 53.5 kg/m^{2}s, both for single-phase liquid flow as well as for single-phase superheated vapour flow, a value of the heat transfer coefficient of 400 W/m^{2}K is

obtained (Fig. 3). At the same time, the Reynolds number for vapour is an order of magnitude greater than for a liquid.

For both liquid and vapour, compliance with the Dittus-Boelter correlation [36] is good, with an error limit of less than ±30 % (Fig. 4).

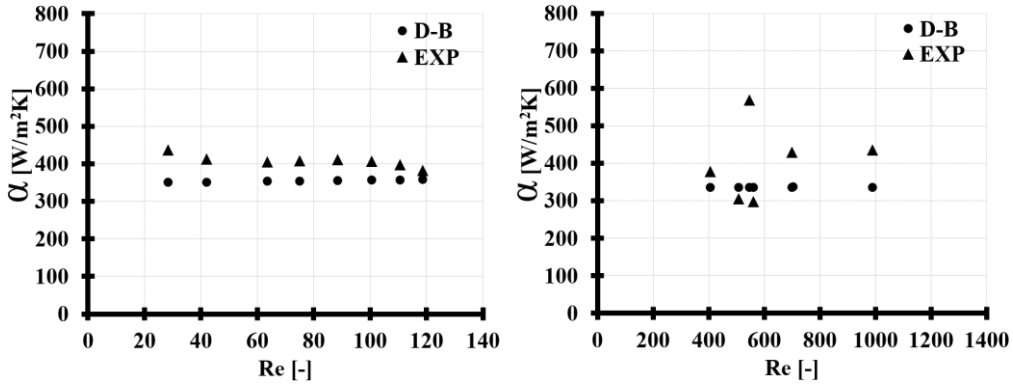

Fig. 3. Average heat transfer coefficient as a function of the Reynolds number for minigap 1.0 mm; left – single-phase liquid flow; right – single-phase vapour flow; EXP – experimental data, D-B – Dittus-Boelter correlation [36]

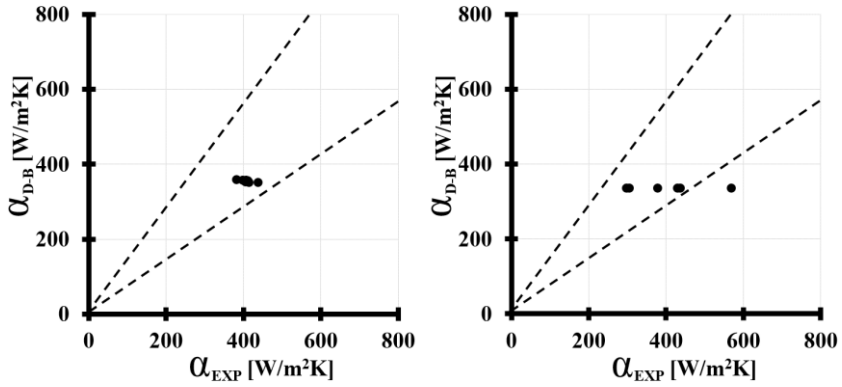

Fig. 4. Comparison of experimental HTC with Dittus-Boelter correlation [36];left – single-phase liquid flow; right – single-phase vapour flow

3.2. Heat transfer and pressure drop during two-phase flow

As can be seen in Figs. 5 and 6, the heat transfer coefficients for two-phase flow are 10 to 20 times higher than for a single phase. The values are measured locally, at the points shown in Fig. 2. In addition, the graphs show a comparison of two minigap thicknesses: 0.5 and 1.0 mm.

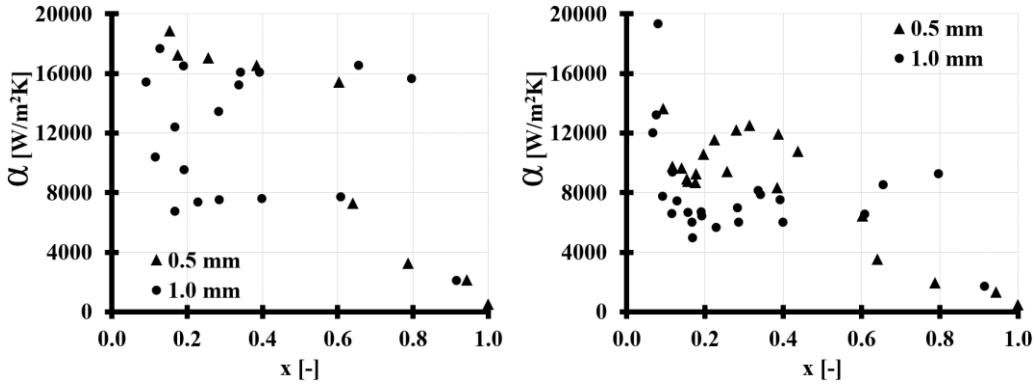

Fig. 5. Local heat transfer coefficient in the initial sector of the examined minigap (up to 41.5 mm from the inlet threshold, points L1 & R1) as a function of the vapour quality

Because the heated and tested part of the section begins just behind the inlet manifold (no distance for stabilisation), the situation in Fig. 5 is connected with inlet effects. For this reason, neither the curve trends nor the interrelationships of minigaps of different thicknesses are legible here. However, it can be seen that on the right side stabilisation occurs faster. It's an effect of the maldistribution phenomena.

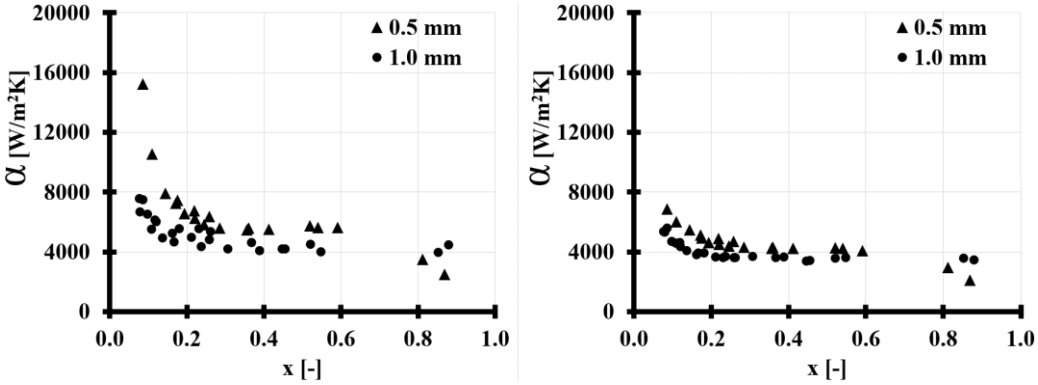

Fig. 6. Local heat transfer coefficient in the central sector of the examined minigap (from 80.5 mm to 119.5 mm from the inlet threshold, points L4 & R4) as a function of the vapour quality

In the central part of the section (Fig. 6), stable flow and heat exchange conditions can be observed. There are also some overall rules noticeable that are consistently repeated in the whole measurement series.

The 0.5 mm minigap exhibits local HTC values about 50% higher compared to 1.0 mm for low and medium vapour qualities. The curve profiles for both minigap thicknesses are the same; they are

shifted relative to each other. In each case, the maximum HTC value occurs for x = 0.1. This is partly consistent with previous authors' observations made for individual minichannels [2]. For x > 0.8, the situation reverses and higher HTC values are shown by the higher minigap thickness. However, a downward HTC trend is visible in this area.

This may be explained as follows: when the minigap thickness decreases, the proportion of the viscosity forces in relation to the inertia forces increases. This effect loses importance when the vapour phase dominates in the flow, which happens for the high vapour qualities.

The decrease in HTC is caused by the fact that for vapour quality above 0.8, local dry-outs occur (see Fig. 7). It can be seen that dry-out starts to occur near the outlet and then develops covering almost half of the minigap area. In these places, the heat exchange takes place between the channel wall and the vapour, which gives local HTC values an order of magnitude lower.

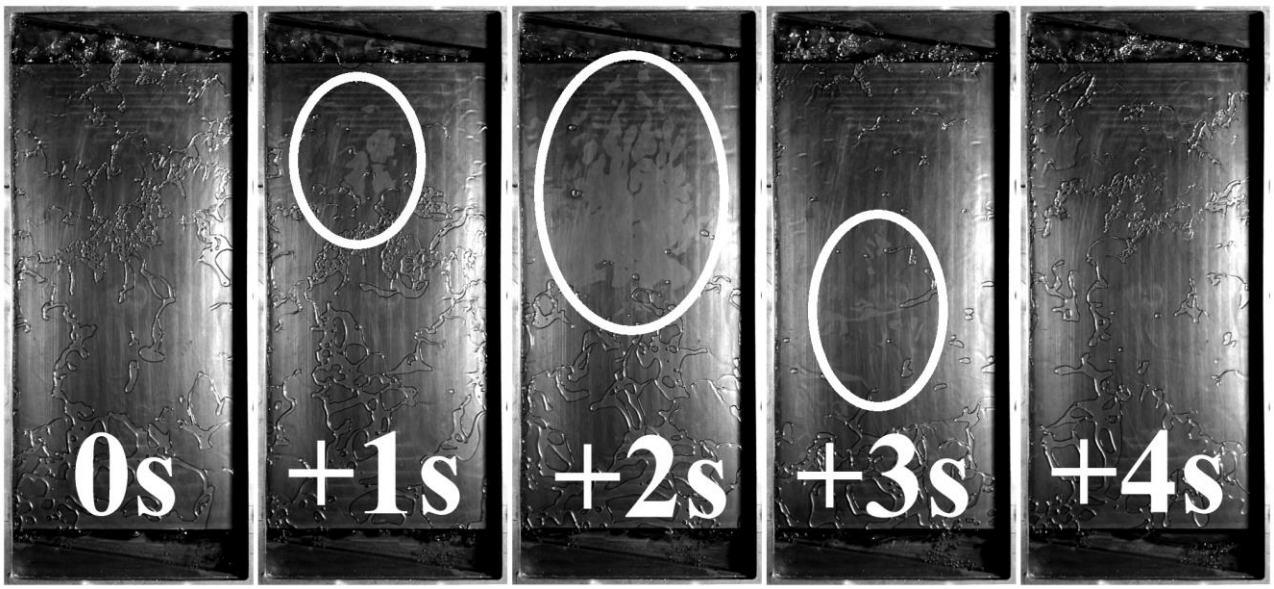

Fig. 7. The example of the local dry-out near the outlet of the 1 mm minigap, G = 4.2 kg/m^{2}s $\dot{q}$ = 9299.1 W/m^2, T_{sat} = 80.3ºC, x_{in} = 0.31, x_{out} = 0.83

In the final part of the section (Fig. 8), the stable conditions are still visible. A significant change occurs at point L6, which is located closest to the outlet. The heat transfer coefficients are the highest here in terms of absolute values, the largest is the difference between the 0.5 mm and 1.0 mm minigap, reaching 100%.

Along the entire section length, the smoother nature of the HTC curves can be seen on the right side of the section. The differences between the right and left sides are most vivid in the areas at the edge of the minigap, just after the inlet threshold and just before the outlet threshold.

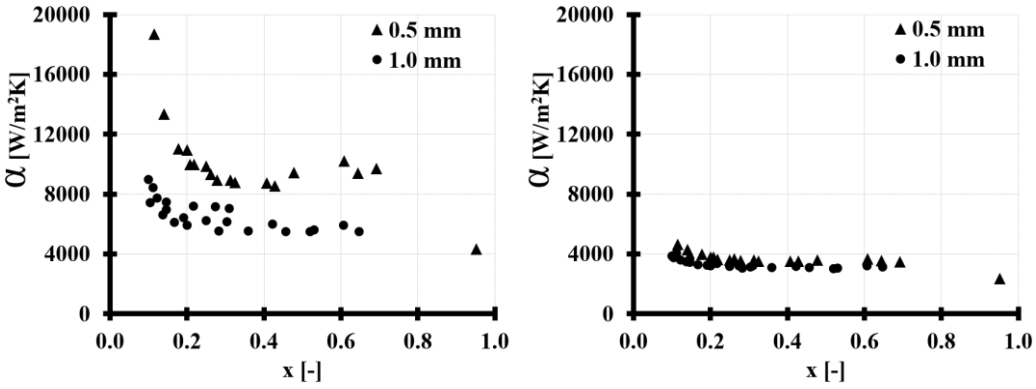

Fig. 8. Local heat transfer coefficient in the final sector of the examined minigap (from 158.5 mm to 197.5 mm from the inlet threshold, points L6 & R6) as a function of the vapour quality

Averaging the HTC values over the entire section essentially confirms all previous observations, as can be seen in Fig. 9. There is a maximum of the HTC for x = 0.1 (in a few cases, these values are very high and have to be treated as errors resulting from the inaccuracy of ΔT estimation). For x in the range of 0.2 to 0.6 the situation is stabilised with a 50% higher HTC for a 0.5 mm minigap. Above x = 0.8, the 1.0 mm minigap is favourable but the HTC shows a downward trend.

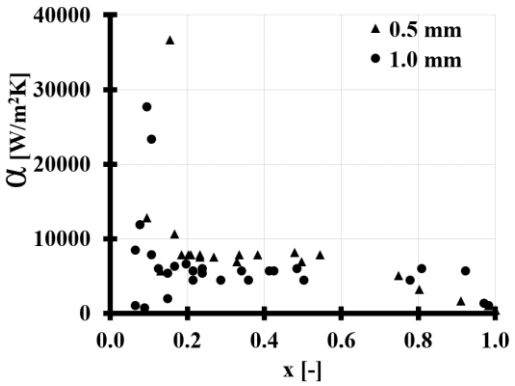

Fig. 9. Average heat transfer coefficient in the minigap from Figs. 5, 6 and 8 as a function of the vapour quality

As expected, along with the reduction of the minigap thickness and cross-section there is an increase in the pressure drop (caused by increasing flow resistance). As shown in Fig. 10, pressure drops for

both minigaps look quantitatively similar as a function of the mass flow rate and as a function of the Reynolds number (where the mass flow rate is the main component).

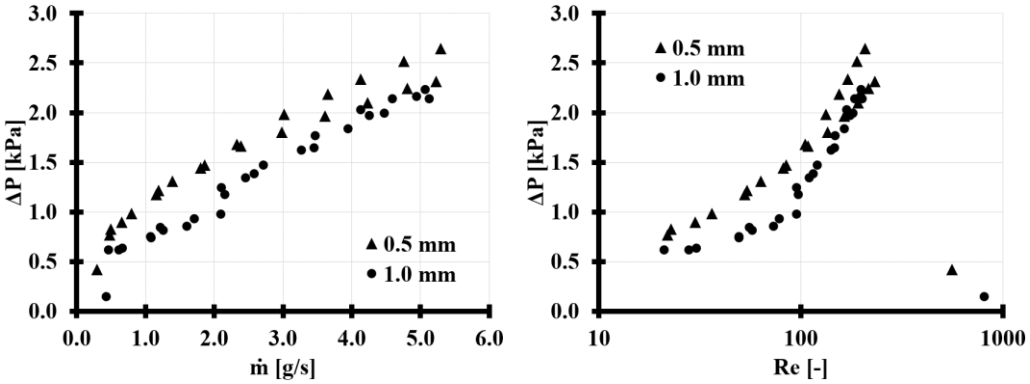

Fig. 10. Pressure drop as a function of the mass flow rate and Reynolds number

On the graph of the function Re, the last two points representing the area of the superheated vapour are worth paying attention to. A sudden increase in Re (by an order of magnitude) after moving to this area indicates a radical decrease in the kinematic viscosity of the working fluid. This results in the relatively low flow resistance of the superheated vapour. The decrease in flow resistance of the two-phase flow is visible with the development of boiling and an increasing x, as can be seen in Fig. 11.

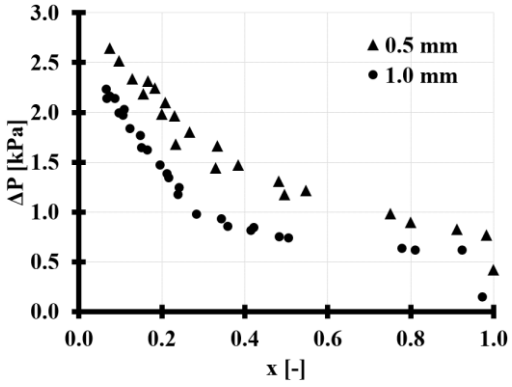

Fig. 11. Pressure drop as a function of the vapour quality

Except for the analysis with the use of the heat transfer coefficient, another possibility for showing the efficiency of heat exchange and its change with minigap thickness is to use the heat flux received by the working medium from the channel wall. This approach is shown in Fig. 12.

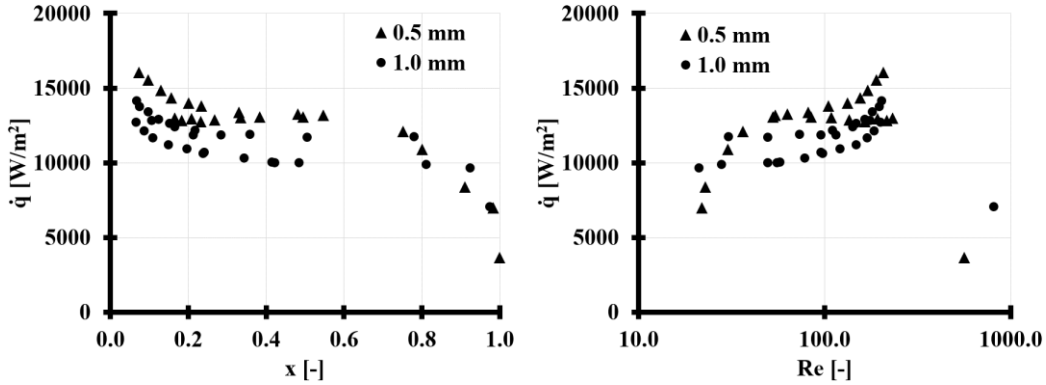

Fig. 12. Heat flux taken from the minigap wall by the working medium as a function of vapour quality (left) and Reynolds number (right)

In the approach using the function of x, very similar trends can be seen. The maximum heat received is for a vapour quality of about 0.1. Above x = 0.2 there is a stabilisation area. Starting from x = 0.8, a decrease in $\dot{q}$ can be noticed. For the range of low and medium vapour qualities, an advantage of about 50% for the 0.5 mm minigap is visible, for x > 0.8 the advantage in this approach is difficult to indicate.

As a function of the Reynolds number, there is an upward trend in the heat flux received. The situation radically changes when transiting to the area of superheated vapour due to the much worse conditions of heat exchange between the wall and the vapour.

Under the presented measurement conditions, a strong increase in the average heat transfer coefficient is visible along with the increase in the heat flux supplied to the wall (Fig. 13, left). This means that for higher heat fluxes, the heat exchange process is more effective (wall superheating does not increase proportionally). The change of HTC as a function of the wall superheating (the temperature difference between the wall temperature and the saturation temperature) is shown in Fig. 13, right. Decreasing HTC with increasing temperature difference is the expected result.

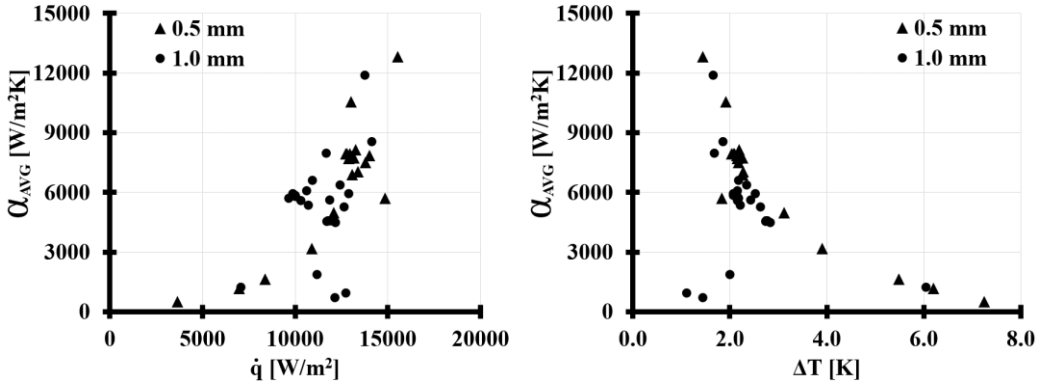

Fig. 13. Heat transfer coefficient as a function of heat flux taken from the channel wall (left) and of the wall superheating (right)

From Fig. 14, good agreement of the experimental data with the correlation for vapour quality of 0.2 and above can be seen. The maximum HTC value, always found in the experiment for x = 0.1, is not reflected in the correlation.

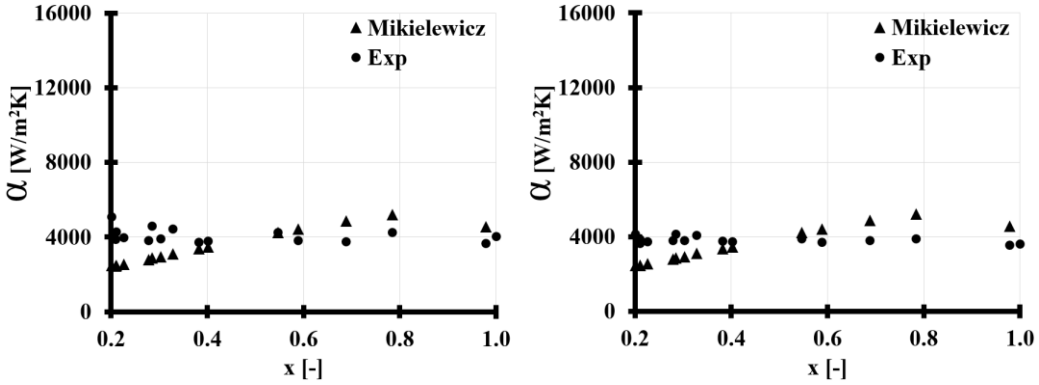

Fig. 14. Comparison of the experimental results with the Mikielewicz correlation [37] for the middle sector of the measuring section (points L3 – left & R4 – right); minigap 1.0 mm, T_{sat} = 80.4˚C, T_{wall} = 90˚C, P_{in} = 111.1 kPa

The comparison in Fig. 15 gives results far from perfect – only about 50% of the measuring points are lying within the 30% error border. However, it should be borne in mind that the number of measuring points for the low vapour qualities is much higher (the compliance is worse in this range) compared to the range for medium and high x values (where the compliance is good).

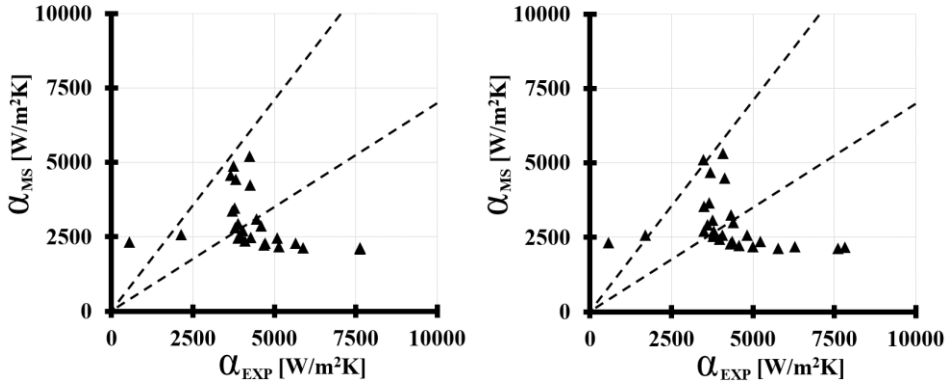

Fig. 15. Comparison of the experimental data with the Mikielewicz correlation [37]

Comparison of the experimental results with the Mikielewicz correlation as a function of the minigap length (Fig. 16) indicates that the quantitative agreement depends on the mass flux of the medium and it's best for relatively low flows. At the same time, there is always a significant discrepancy at the first measuring point, located just over the threshold of the inlet manifold. This is probably the effect of the lack of stabilisation and the occurrence of inlet effects, already discussed for Fig. 5. In addition, apart from a larger or smaller shift, the trend of the curves is consistent. The exception is the highest G value where a quantitative discrepancy exceeding 300% and a chaotic distribution of experimental points occurs for at least half the length of the section.

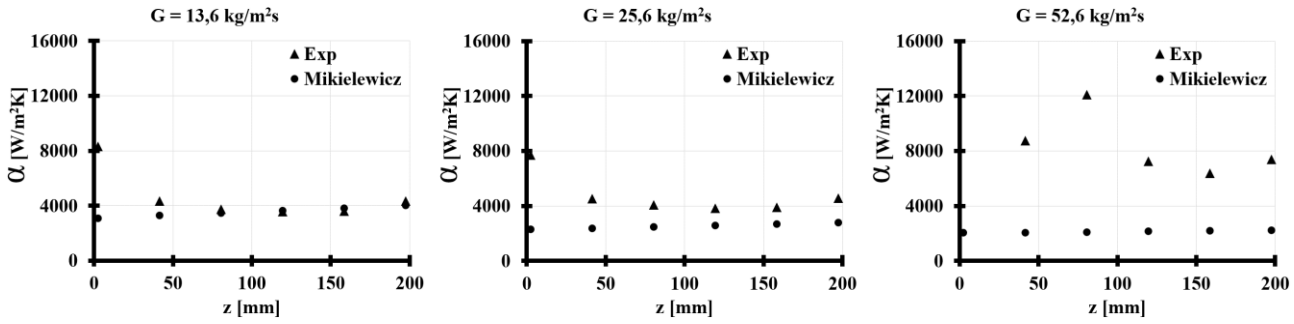

Fig. 16. Comparison of the experimental results with the Mikielewicz correlation [37] as a function of the minigap length; minigap 1.0 mm, T_{sat} = 80.4˚C, T_{wall} = 90˚C, P_{in} = 111.1 kPa

3.3. Minigap vs minichannel multiport

Figures 17, 18 and 19 describe the characteristics of heat exchange in both variants of the heat exchanger. Figure 17 shows the transferred heat flux as a function of mass flux for different temperatures of the heat exchanger wall and saturation temperature of about 71˚C. In almost every

case, the predominance of the minichannels over the minigap is visible, except for the lowest mass fluxes. This difference goes up to 250% in the tested mass flux range. This is accurately reflected by the local heat transfer coefficient (HTC). Figures 18 and 19 show the local HTC curves as a function of the vapour quality for points on the heat exchanger wall according to Fig. 2. The same difference in favour of the minichannels is visible here.

In the presented studies, only one side of the test section is heated, the other is transparent of the need for flow visualisation. In this configuration, the minichannels form fins. Not only the bottom parts but also the sides of the channels participate in supplying the heat to the working fluid. In relation to the minigap, this creates a developed surface, despite the same active cross-section area. Since the minichannel section does not show a significant increase in flow resistance, it can be considered more favourable from the heat exchange point of view. However, a much easier production and a much lower possibility of blocking by impurities make the minigap geometry favourable (these are important issues from the possible implementations point of view).

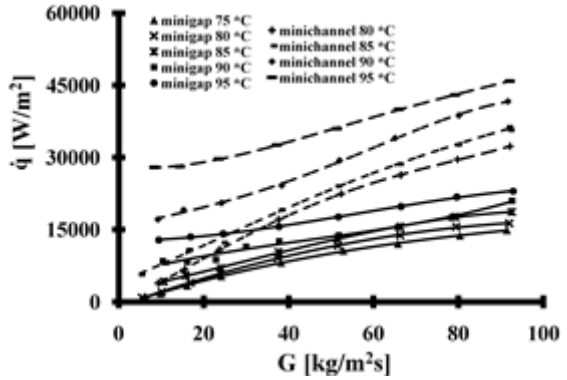

Fig. 17. Heat flux transported in the test section – comparison of 0.5 mm thick minigap (continuous line) with a set of 50 1x1 mm minichannels (dotted line) for various wall temperatures

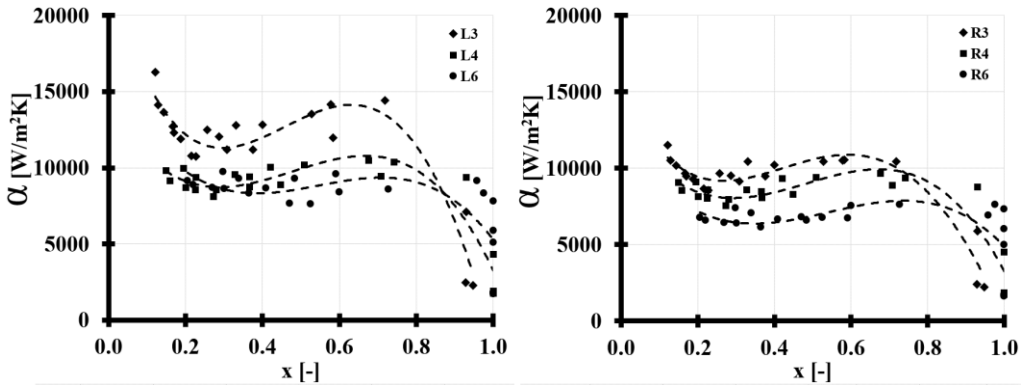

Fig. 18. Local heat transfer coefficient for a set of 50 1x1 mm minichannels; left and right side of the heat exchanger; average T_{sat} = 70.5˚C, average T_{wall} = 90˚C

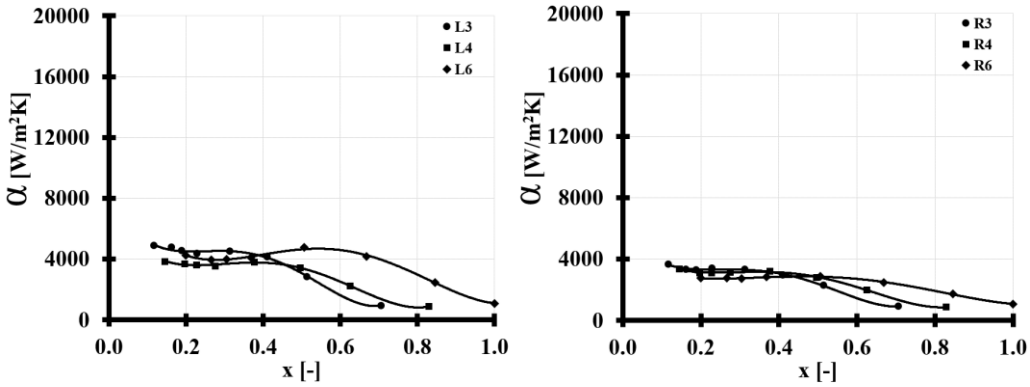

Fig. 19. Local heat transfer coefficient for 0.5 mm minigap; left and right side of the heat exchanger; average T_{sat} = 71.2˚C, average T_{wall} = 90˚C

Besides, the HTC – in both cases – are higher for the left side of the heat exchanger. The reason is in the flow specifics through the heat exchanger equipped with trapezoidal manifolds. On visual tests, in each case, the flow orientation is closer to the left side of the heat exchanger. This is related to the flow maldistribution [14]. On the right, there are more blocked channels [21] and reversed flows occur.

In all the cases discussed, the HTC curve as a function of the vapour quality adopts a distribution similar to the "M-shape" as reported in [5] and [6] for single minichannels. Extremes for x = 0.1 and around x = 0.6 are clearly visible. As in the aforementioned reports, the reasons should be seen at the points of changing the boiling mechanism/flow structure.

As shown in Fig. 20, the change in pressure drop is relatively small. It can be seen that above a mass flow rate of 2 g/s, the minigap begins to show slightly lower flow resistance than the minichannel section.

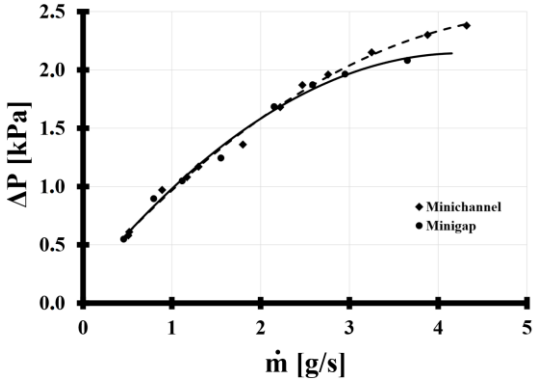

Fig. 20. Pressure drop – comparison of a 0.5 mm thick minigap (continuous line) with a set of 50 1x1 mm minichannels (dotted line) as a function of mass flow rate

3.4. A heat transfer intensification attempt

Keeping in mind the practical aspects of possible applications, a simple, passive method of heat transfer intensification was chosen consisting of mechanical modification of the heat exchange surface. The aim was to create additional places for nucleation (Fig. 21, left) and achieve a more even distribution of the working fluid (Fig. 21, right).

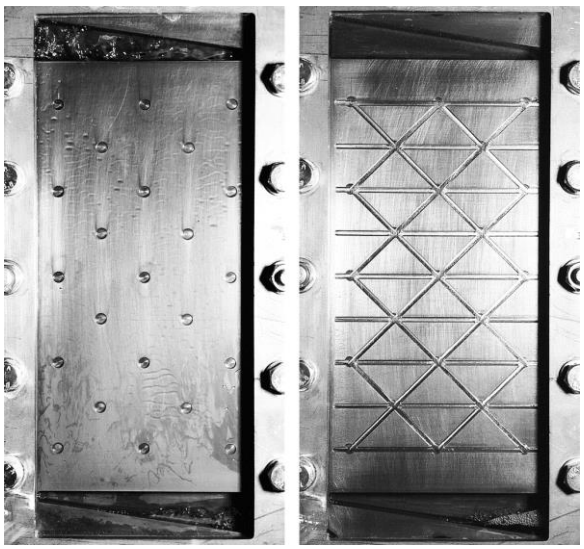

Fig. 21. Variants of 1 mm minigap surface modification; left: 23 dimples, diameter = 4 mm, depth = 0.2mm; right: cross-cuts, width = 3 mm, depth = 0.2 mm

Figures 22 and 23 show the local HTC as a function of vapour quality. In both cases, the middle part of the measuring section was selected to obtain a steady flow, with no influence from the manifolds, inlet and outlet.

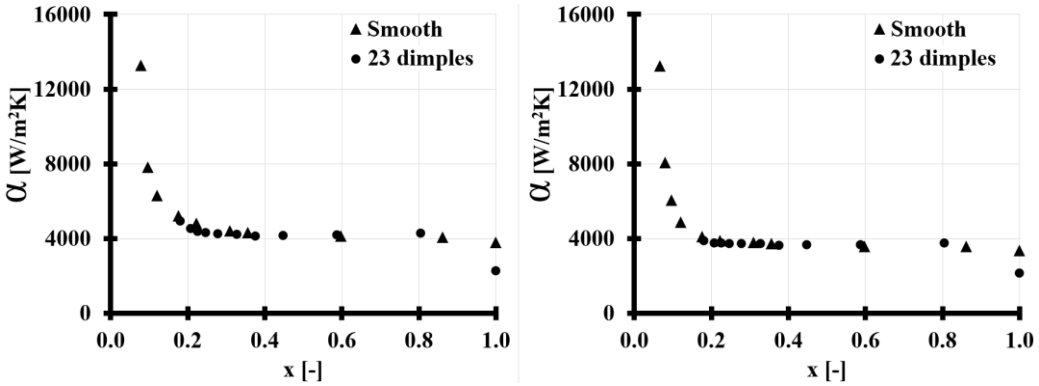

Fig. 22. Flow boiling intensification, variant 1: 23 dimples on the surface of a 1 mm minigap; measuring points L4 – left and R4 – right.

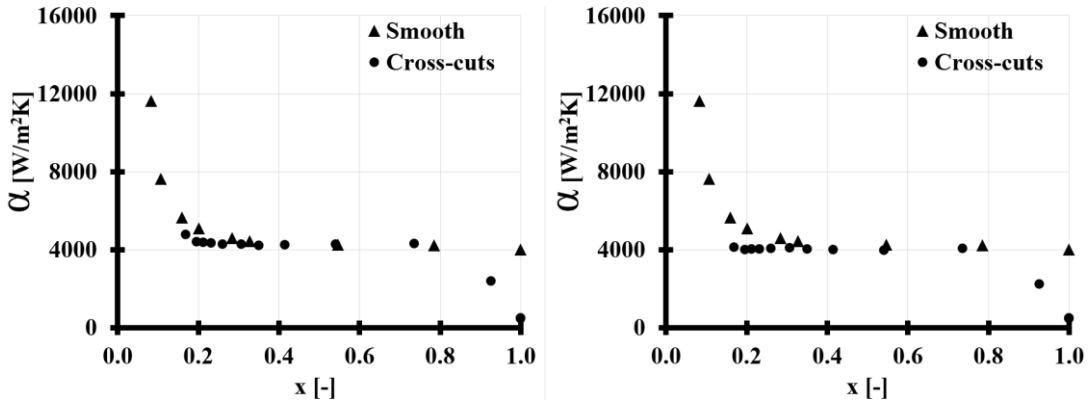

Fig. 23. Flow boiling intensification, variant 2: cross-cuts on the surface of a 1 mm minigap; measuring points L3 – left and R3 – right

As can be seen, in both cases there is no significant intensification effect in the form of increasing the local heat transfer coefficient. However, there is a change in the HTC curve trend for the case of cross-cuts. The characteristic maximum for low vapour qualities does not appear. This brings the trend closer to the Mikielewicz correlation [37] and may indicate that this modification affects the even distribution of the working medium.

As shown in Fig. 24, the first variant of intensification did not substantially change the pressure drop. For the second variant, the pressure drop is even a bit smaller which seems to confirm the conclusion about a more even distribution of the working fluid. It is also confirmed by visual observation of the flow structures.

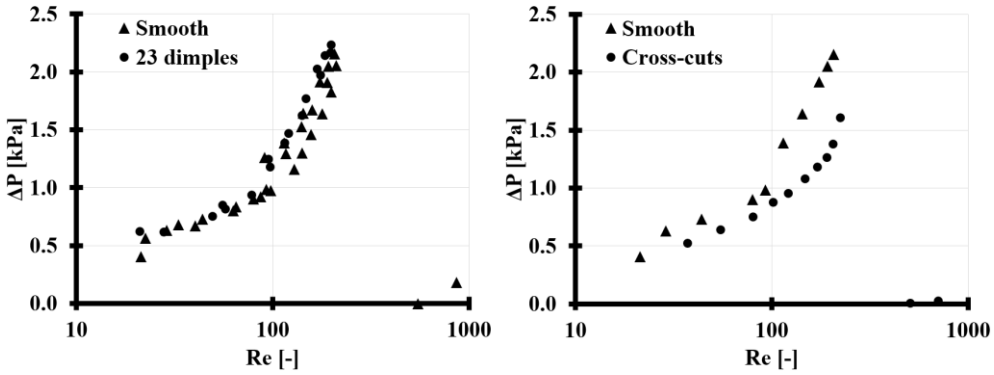

Fig. 24. Pressure drop as a function of the Reynolds number for both variants of intensification

Figure 25 shows the flow visualization for the smooth minigap during the boiling. The flow generally tends to orient itself closer to the left edge of the minigap. This is also confirmed in quantitative

results where the left side is always characterized by greater HTC. For the smooth minigap, the flow path of the vapour bubbles becomes curved. The arrow indicates the bubble which develops and moves towards the outlet. It can be seen that flow adopts the shape of the letter "S", with two distinct focal points of reversed flow.

Figure 26 shows the flow visualization for the modified minigap during the boiling. The solid line shows the front of the generated bubbles that are moving toward the outlet manifold. The effect of mechanical modification of the heat exchange surface (cross-cuts) is visible. For the modified minigap, the vapour bubbles move upwards along a straight line, although the shift of the flow axis towards the left edge of the minigap is visible. The cross-cut channels are a place of more intense bubble nucleation, and they also create a path for the vapour that the vapour follows, evenly filling the entire gap area and so reducing the maldistribution phenomenon.

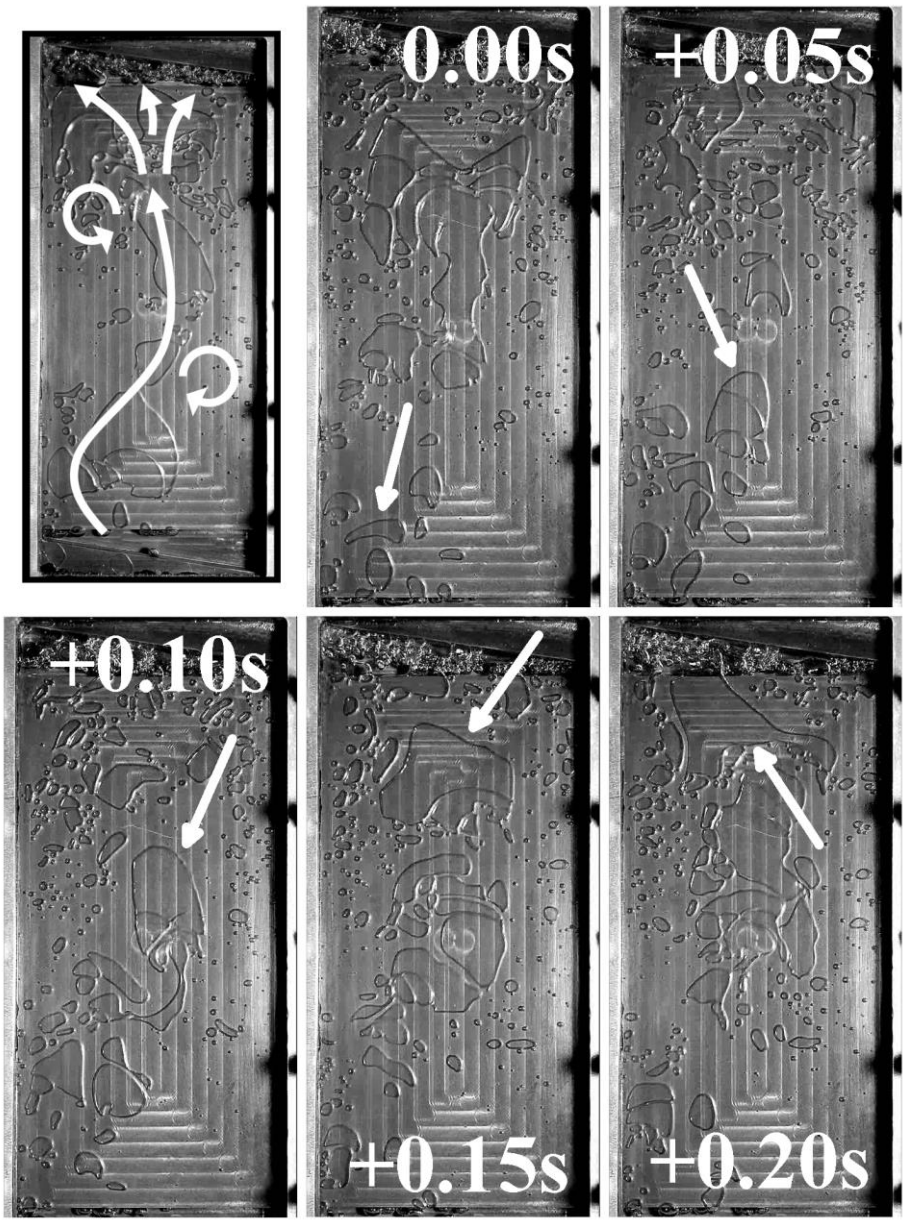

Fig. 25. The flow distribution in a smooth minigap section. The top left corner image shows the general path of fluid, other images show 5 different instants of time.

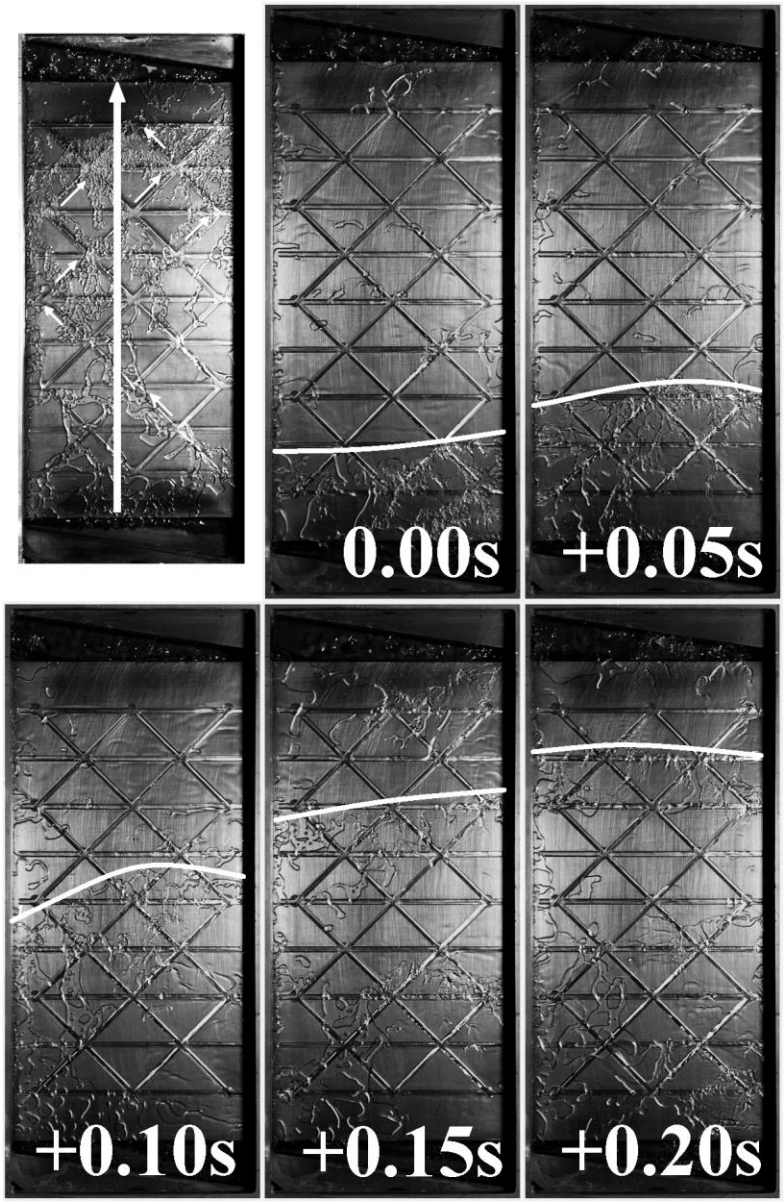

Fig. 26. The flow distribution in a cross-cut minigap section. The top left corner image shows the general path of fluid, other images show 5 different instants of time.

4. Conclusions

a) Both for single-phase heat exchange and for flow boiling, the obtained HTC values are consistent by an order of magnitude, with literature correlations. In the case of flow boiling, the biggest discrepancy concerns the low vapour qualities, but this may be caused by the inlet effects and flow maldistribution. This conclusion results from the observation that the appropriate minigap surface modification changes this effect, along with visible better flow uniformity.

b) The type of manifolds and the inlet and outlet configuration cause maldistribution phenomena on the heat exchange surface. The difference between the left and right side of the section is significant as well as the disturbances near the inlet and outlet.

c) The value of the local heat transfer coefficient increases as the thickness of the minigap decreases. The heat transfer coefficient is also higher for a minichannel multiport than for a minigap of the same cross-section area.

d) The pressure drop is relatively small and changes quite slightly. A 25% increase is visible when the thickness of the minigap decreases two times. The pressure drop slightly increases for a minichannel multiport compared to a minigap at higher mass flow rates.

e) An attempt to intensify heat transfer by simply modifying the minigap surface has not resulted in a significant increase in HTC. However, one of the variants has an impact on the nature of the working fluid distribution, causing a change in the trend of the HTC curve and a decrease in flow resistance of about 25%. This confirms the authors' previous observations for minichannels [36] that the intensification of the heat transfer in flow boiling is hard to obtain through simple passive methods.

5. Literature

[1] D.B. Tuckerman, R.F.W. Pease, High-performance heat sinking for VLSI, IEEE Electron Device Lett. 2 (1981) 126–129. doi:10.1109/EDL.1981.25367.

[2] D. Mikielewicz, M. Klugmann, J. Wajs, Experimental Investigation of M-Shape Heat Transfer Coefficient Distribution of R123 Flow Boiling in Small-Diameter Tubes, Heat Transf. Eng. 33 (2012) 584–595. doi:10.1080/01457632.2012.630245.

[3] M. Piasecka, B. Maciejewska, Heat transfer coefficient during flow boiling in a minichannel at variable spatial orientation, Exp. Therm. Fluid Sci. 68 (2015) 459–467. doi:10.1016/j.expthermflusci.2015.05.005.

[4] M. Piasecka, Impact of selected parameters on refrigerant flow boiling heat transfer and

pressure drop in minichannels, Int. J. Refrig. 56 (2015) 198–212. doi:10.1016/j.ijrefrig.2015.03.024.

[5] D. Mikielewicz, J. Wajs, R. Andrzejczyk, M. Klugmann, Pressure drop of HFE7000 and HFE7100 during flow condensation in minichannels, Int. J. Refrig. 68 (2016) 226–241. doi:10.1016/j.ijrefrig.2016.03.005.

[6] M. Piasecka, K. Strąk, B. Maciejewska, Calculations of Flow Boiling Heat Transfer in a Minichannel Based on Liquid Crystal and Infrared Thermography Data, Heat Transf. Eng. 38 (2017) 332–346. doi:10.1080/01457632.2016.1189272.

[7] K. Strąk, M. Piasecka, B. Maciejewska, Spatial orientation as a factor in flow boiling heat transfer of cooling liquids in enhanced surface minichannels, Int. J. Heat Mass Transf. 117 (2018) 375–387. doi:10.1016/j.ijheatmasstransfer.2017.10.019.

[8] A.K.M.M. Morshed, F. Yang, M. Yakut Ali, J.A. Khan, C. Li, Enhanced flow boiling in a microchannel with integration of nanowires, Appl. Therm. Eng. 32 (2012) 68–75. doi:10.1016/j.applthermaleng.2011.08.031.

[9] D. Mikielewicz, J. Wajs, Possibilities of heat transfer augmentation in heat exchangers with minichannels, 24 (2017) 133–140.

[10] L. ming Pan, R. gang Yan, H. jie Huang, H. He, P. fei Li, Experimental study on the flow boiling pressure drop characteristics in parallel multiple microchannels, Int. J. Heat Mass Transf. 116 (2018) 642–654. doi:10.1016/j.ijheatmasstransfer.2017.09.033.

[11] A.S. Dalkılıç, C. Özman, K. Sakamatapan, S. Wongwises, Experimental investigation on the flow boiling of R134a in a multi-microchannel heat sink, Int. Commun. Heat Mass Transf. 91 (2018) 125–137. doi:10.1016/j.icheatmasstransfer.2017.12.008.

[12] L.S. Maganti, P. Dhar, T. Sundararajan, S.K. Das, Heat spreader with parallel microchannel configurations employing nanofluids for near–active cooling of MEMS, Int. J. Heat Mass Transf. 111 (2017) 570–581. doi:10.1016/j.ijheatmasstransfer.2017.04.032.

[13] H. Li, P. Hrnjak, Quantification of liquid refrigerant distribution in parallel flow microchannel heat exchanger using infrared thermography, Appl. Therm. Eng. 78 (2015) 410–418. doi:10.1016/j.applthermaleng.2015.01.003.

[14] P. Dąbrowski, M. Klugmann, D. Mikielewicz, Selected studies of flow maldistribution in a minichannel plate heat exchanger, Arch. Thermodyn. 38 (2017) 135–148. doi:10.1515/aoter-2017-0020.

[15] M. Klugmann, P. Dabrowski, D. Mikielewicz, Pressure drop related to flow maldistribution in a model minichannel plate heat exchanger, Arch. Thermodyn. 39 (2018) 123–146. doi:10.1515/aoter-2018-0015.

[16] V. Singh, H. Kumar, S.S. Sehgal, R. Kukreja, Effect of Plenum Shape on Thermohydraulic Performance of Microchannel Heat Sink, J. Inst. Eng. Ser. C. (2019). doi:10.1007/s40032-019-00515-z.

[17] A.T. Wijayanta, T. Miyazaki, S. Koyama, Refrigerant distribution in horizontal headers with downward minichannel-branching conduits: Experiment, empirical correlation and two-phase flow pattern map, Exp. Therm. Fluid Sci. 81 (2017) 430–444. doi:10.1016/j.expthermflusci.2016.09.011.

[18] A.T. Wijayanta, T. Miyazaki, S. Koyama, Liquid-vapor phase distribution in horizontal headers with upward minichannel-branching conduits, Exp. Therm. Fluid Sci. 76 (2016) 264–274. doi:10.1016/j.expthermflusci.2016.03.021.

[19] A.A.Y. Al-Waaly, M.C. Paul, P. Dobson, Liquid cooling of non-uniform heat flux of a chip circuit by subchannels, Appl. Therm. Eng. 115 (2017) 558–574. doi:10.1016/j.applthermaleng.2016.12.061.

[20] V. Manoj Siva, A. Pattamatta, S.K. Das, Effect of flow maldistribution on the thermal performance of parallel microchannel cooling systems, Int. J. Heat Mass Transf. 73 (2014) 424–428. doi:10.1016/j.ijheatmasstransfer.2014.02.017.

[21] P. Dąbrowski, M. Klugmann, D. Mikielewicz, Channel Blockage and Flow Maldistribution

during Unsteady Flow in a Model Microchannel Plate heat Exchanger, J. Appl. Fluid Mech. 12 (2019) 1023–1035. doi:10.29252/jafm.12.04.29316.

[22] J. Kim, J.H. Shin, S. Sohn, S.H. Yoon, Analysis of non-uniform flow distribution in parallel micro-channels, J. Mech. Sci. Technol. 33 (2019) 3859–3864. doi:10.1007/s12206-019-0729-8.

[23] M. Klugmann, P. Dąbrowski, D. Mikielewicz, Flow Boiling in Minigap in the Reversed Two-Phase Thermosiphon Loop, Energies. 12 (2019) 3368. doi:10.3390/en12173368.

[24] J. Mathew, P.S. Lee, T. Wu, C.R. Yap, Experimental study of flow boiling in a hybrid microchannel-microgap heat sink, Int. J. Heat Mass Transf. 135 (2019) 1167–1191. doi:10.1016/j.ijheatmasstransfer.2019.02.033.

[25] A. Tamanna, P.S. Lee, Flow boiling heat transfer and pressure drop characteristics in expanding silicon microgap heat sink, Int. J. Heat Mass Transf. 82 (2015) 1–15. doi:10.1016/j.ijheatmasstransfer.2014.11.047.

[26] T. Alam, P.S. Lee, C.R. Yap, L. Jin, A comparative study of flow boiling heat transfer and pressure drop characteristics in microgap and microchannel heat sink and an evaluation of microgap heat sink for hotspot mitigation, Int. J. Heat Mass Transf. 58 (2013) 335–347. doi:10.1016/j.ijheatmasstransfer.2012.11.020.

[27] D. Lorenzini, C. Green, T.E. Sarvey, X. Zhang, Y. Hu, A.G. Fedorov, M.S. Bakir, Y. Joshi, Embedded single phase microfluidic thermal management for non-uniform heating and hotspots using microgaps with variable pin fin clustering, Int. J. Heat Mass Transf. 103 (2016) 1359–1370. doi:10.1016/j.ijheatmasstransfer.2016.08.040.

[28] P. Dąbrowski, The Mitigation of the Flow Maldistribution in Minichannel and Minigap Heat Exchangers by Introducing Threshold in the Manifolds, J. Appl. Fluid Mech. 13 (2020).

[29] G.D. Xia, J. Jiang, J. Wang, Y.L. Zhai, D.D. Ma, Effects of different geometric structures on fluid flow and heat transfer performance in microchannel heat sinks, Int. J. Heat Mass Transf. 80 (2015) 439–447. doi:10.1016/j.ijheatmasstransfer.2014.08.095.

[30] T. Alam, P.S. Lee, C.R. Yap, L. Jin, K. Balasubramanian, Experimental investigation and flow visualization to determine the optimum dimension range of microgap heat sinks, Int. J. Heat Mass Transf. 55 (2012) 7623–7634. doi:10.1016/j.ijheatmasstransfer.2012.07.080.

[31] A. Tamanna, P.S. Lee, Flow boiling heat transfer and pressure drop characteristics in expanding silicon microgap heat sink, Int. J. Heat Mass Transf. 82 (2015) 1–15. doi:10.1016/j.ijheatmasstransfer.2014.11.047.

[32] J. Zhou, X. Zhao, X. Ma, Z. Du, Y. Fan, Y. Cheng, X. Zhang, Clear-days operational performance of a hybrid experimental space heating system employing the novel mini-channel solar thermal & PV/T panels and a heat pump, Sol. Energy. 155 (2017) 464–477. doi:10.1016/j.solener.2017.06.056.

[33] J. Wajs, D. Mikielewicz, E. Fornalik-Wajs, Thermal performance of a prototype plate heat exchanger with minichannels under boiling conditions, J. Phys. Conf. Ser. 745 (2016) 032063. doi:10.1088/1742-6596/745/3/032063.

[34] C. Pistoresi, Y. Fan, L. Luo, Numerical study on the improvement of flow distribution uniformity among parallel mini-channels, Chem. Eng. Process. Process Intensif. 95 (2015) 63–71. doi:https://doi.org/10.1016/j.cep.2015.05.014.

[35] C. Amador, A. Gavriilidis, P. Angeli, Flow distribution in different microreactor scale-out geometries and the effect of manufacturing tolerances and channel blockage, Chem. Eng. J. 101 (2004) 379–390. doi:10.1016/j.cej.2003.11.031.

[36] D. Mikielewicz, M. Klugmann, J. Wajs, Flow boiling intensification in minichannels by means of mechanical flow turbulising inserts, Int. J of Th. Sc. Vol. 65 (2013) 79-91. doi: 10.1016/j.ijthermalsci.2012.10.002

[37] B. Jakubowska, D. Mikielewicz, M. Klugmann, Experimental study and comparison with predictive methods for flow boiling heat transfer coefficient of HFE7000, Int. J. of Heat and Mass Tr. 142 (2019) 1-15. doi:10.1016/j.ijheatmasstransfer.2019.06.063

Acknowledgement

The work presented in this paper was funded from the National Science Centre Poland research project No. UMO-2015/19/D/ST8/03201 in the years 2016–2019 and from the National Science Centre, Poland research project No. 2017/27/N/ST8/02785 in the years 2018-2020.